Advanced Composite Materials
Publication details, including instructions for authors and subscription information:
http://www.tandfonline.com/loi/tacm20

Effect of zigzag damage extension mechanism on fracture toughness of cross-ply laminated carbon/carbon composites

Mohamed S. Aly-Hassan , Hiroshi Hatta & Shuichi Wakayama

Version of record first published: 02 Apr 2012.

To cite this article: Mohamed S. Aly-Hassan , Hiroshi Hatta & Shuichi Wakayama (2003): Effect of zigzag damage extension mechanism on fracture toughness of cross-ply laminated carbon/carbon composites , Advanced Composite Materials, 12:2-3, 223-236

To link to this article: http://dx.doi.org/10.1163/156855103772658579

Adv. Composite Mater., Vol. 12, No. 2-3, pp. 223–236 (2003)

Also available online - www.vsppub.com

Effect of zigzag damage extension mechanism on fracture toughness of cross-ply laminated carbon/carbon composites

MOHAMED S. ALY-HASSAN [1,*], HIROSHI HATTA [2] and SHUICHI WAKAYAMA [1]

[1] *Department of Mechanical Engineering, Graduate School of Engineering, Tokyo Metropolitan University, 1-1 Minami-Ohsawa, Hachioji, Tokyo 192-0397, Japan*
[2] *Division of Space Propulsion, The Institute of Space and Astronautical Science, 3-1-1 Yoshinadai, Sagamihara, Kanagawa 229-8510, Japan*

Received 5 July 2002; accepted 16 December 2002

Abstract—The fracture behavior and damage mechanisms of a cross-ply-laminated carbon/carbon (C/C) composite was investigated using compact tension (CT) and double-edge-notched (DEN) geometry. The C/C composite exhibited an interesting 'zigzag cracking' during growth of the damage in the 0° plies. At the same time, a straight crack extension was formed in the 90° plies. This zigzag crack proceeded in the following order: at first, vertical splits formed, then micro-cracks between the splits, and finally a connecting unstable crack formed. A stable/unstable regime of zigzag cracking was repeated for several cycles until the final failure. An R-curve was determined, taking this cracking extension into account. The R-curve demonstrated that the high-fracture toughness of the cross-ply laminated C/C composites could be attributed to the zigzag cracking characteristics. Then, the DEN results were compared with the R-curve behavior. This comparison showed that the DEN occurred at the initial value of the R-curve obtained when the micro-crack growth length was regarded as the crack tip.

Keywords: Carbon/carbon composites; splitting; micro-cracks; zigzag crack; R-curve; fracture toughness criterion; microscopy observations.

1. INTRODUCTION

Carbon/carbon composites, C/Cs, have received increasing attention in recent years as potential high-temperature materials for advanced applications [1–3]. This

*To whom correspondence should be addressed at Hatta Laboratory, Division of Space Propulsion, The Institute of Space and Astronautical Science, 3-1-1 Yoshinadai, Sagamihara, Kanagawa 229-8510, Japan. E-mail: aly-has@gawab.com

increase in attention arose mainly due to the unique properties of C/Cs. High fracture toughness is an important advantage of C/Cs [4–6]. Compared with monolithic ceramics, C/Cs possess nearly one order higher fracture toughness [7].

Many attempts have been made to identify the damage processes and toughening mechanisms of C/Cs [8–12]. According to recent literature [10–12], it has been widely accepted that the ability of C/Cs to redistribute stresses near notch tips is due to the shear band formation mechanism. This shear damage band extends perpendicular to the notch direction under mode I remote loading. Such damage emanates from the edge of a notch and leads to the reduction of stress concentration ahead of the notch. This damage mechanism enhances crack extension resistance by shielding the crack tip from the applied load. The low shear/tensile strength ratio and weak fiber/matrix interface of C/Cs [8] are thought to be responsible for this behavior. However, the shear bands have rarely been clearly observed in C/Cs on either the microscopic or the macroscopic scale [13, 14]. Only in the case of two-dimensionally reinforced (2D) C/Cs with a filler addition (carbon blacks and colloidal graphite), have the shear bands been observed microscopically [15].

A better understanding of the evolution of damage within C/Cs is necessary in order to clarify the source mechanisms of notch insensitivity; such an explanation would then help to improve structural performance. In the present study, the process of damage development in 2D-C/C was clarified to better understand high fracture toughness behavior and notch insensitivity. Compact tension and double-edge-notch tests were carried out in cross-ply laminated C/Cs, and the crack extension resistance (R-) curve behavior was obtained. The R-curve behavior was then related to fracture process.

2. EXPERIMENTAL PROCEDURES

2.1. Materials

The 2D-C/C composites in the present study were produced via a preformed yarn method (Across Co. Ltd., Japan). The 2D-C/Cs were reinforced with high modulus carbon fibers, Torayca® M40 PAN-based, produced by Toray Industries, Inc., Japan. In the preformed yarn method, bundles of the carbon fibers (6K) and powders of matrix precursor (coke and bulk mesophase pitch) were placed into thin nylon sheaths. These sheathed bundles were arranged unidirectionally and stitched together with thin nylon filament in order to produce a UD-preformed sheet. Then, in the present case, sixteen preformed sheets were laminated (crossed over each other) into a symmetric cross-ply stacking sequence, as shown in Fig. 1, to form a green cross-ply C/Cs. Finally, the green body was hot-pressed in a mold at 600°C for carbonization, followed by heat treatment at a temperature of 2000°C for graphitization in an inert atmosphere to yield cross-ply laminated C/Cs. The fiber volume fraction of this C/C composite was about 50% and the mechanical properties are listed in Table 1.

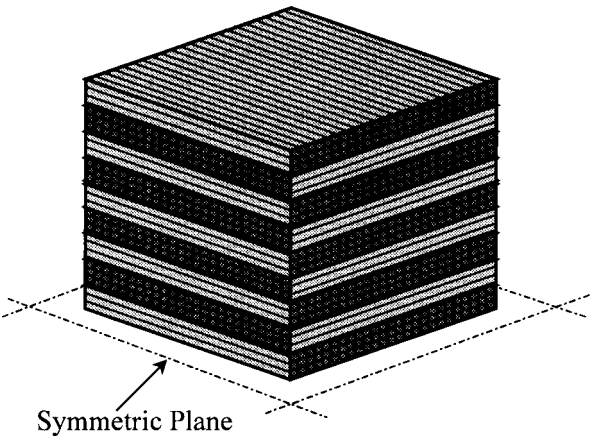

Figure 1. Stacking sequence of cross-ply-laminated C/C composites.

Table 1.
Mechanical and physical properties of used C/C composites

Tensile strength (MPa)	Young's modulus (GPa)	Shear strength (MPa)	Shear modulus (GPa)	Poisson's ratio	Density (g/cm^3)
180.3 ± 5	90.1 ± 3	29 ± 2	5.4	0.026	1.69

2.2. Fracture toughness measurement

The compact tension (CT) tests and tensile tests of double-edge-notch (DEN) specimens were performed using a screw-driven mechanical testing machine (Autograph AG-5000G, Shimadzu Corp., Japan) under a cross-head speed of 0.1 mm/min.

2.2.1. Compact tension test. The CT tests were carried out to obtain the R-curve and to observe damage growth in the cross-ply-laminated C/C composites. The configuration of the CT specimens based on ASTM Standard E-399-72 is given in Fig. 2, where the crack length-to-size ratio, a/W, was set at 0.5. This pre-crack was introduced at first by a diamond wheel with a thickness of 0.4 mm, and then the notch tip was sharpened by a razor blade to a size of 0.1 mm. The C/Cs are known to be insensitive to a notch tip radius within a range of 0–2 mm [14]. In order to observe damage growth in the differently angled plies in the 2D-C/Cs, two types of CT specimen configurations were prepared. The first type had a pre-introduced crack running in the same direction as the fibers in the surface plies, whereas in the other type the cracks run perpendicular to the direction of the surface ply fibers. To observe the process of damage extension by CT test, the samples were polished using diamond-past of 15 μm diameter, degreased in ethanol and cleaned in an ultrasonic bath, dried at room temperature, and then thinly painted white. The damage process was observed from both sides of the specimens using a travelling optical microscope with a magnification of 25 and a CCD camera during

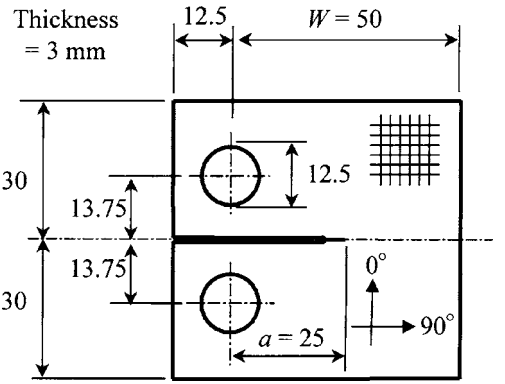

Figure 2. Geometry of the CT specimens.

the CT test. A clip gage (UB-5, Tokyo-Sokki Crop, Japan) was used to measure the crack opening displacement (COD). Two acoustic emission sensors (AE-900M-WE, NF Electric Instruments Crop, Japan) were attached on the CT specimen to provide signals for the damage formation. Compact tension tests were conducted by repeating the loading-unloading cycles.

2.2.2. Double-edge-notch test. Double-Edge-Notch (DEN) specimens (Fig. 3) and smooth specimens were prepared to evaluate the adequacy of the CT results as a fracture toughness criterion. In both specimens, the loading direction was set to the fiber direction of the surface plies. In the DEN specimens, a ratio of total notch length to specimen width ($2a/W$) was fixed at 0.5, and the width of the specimen (W) fell within a range of 8 mm to 24 mm. Tapered aluminum tabs were glued by epoxy adhesive at the grip portions of the DEN and smooth specimens.

2.3. R-curve evaluation

A compliance method was used to determine the crack growth resistance (R-) curve of CT test specimens by applying the linear elastic fracture mechanics to estimate the energy release rate of 2D-C/Cs [13] by the following equation;

$$G_{IR} = \frac{P^2}{2B}\frac{\mathrm{d}c}{\mathrm{d}a}, \tag{1}$$

where P, B, C, and a are the load at each crack increment, CT specimen thickness, compliance measured at the loading point, and crack growth length, respectively. The compliance was determined based on crack opening displacement, COD, at the load axis. Next, energy release rate G_{IR} obtained by equation (1) was converted into the stress intensity factor K_I by use of the following equation:

$$G_{IR} = K_I^2\sqrt{\frac{S_{11}S_{22}}{2}}\left[\sqrt{\frac{S_{22}}{S_{11}}} + \frac{2S_{12} + S_{66}}{2S_{11}}\right]^{1/2}, \tag{2}$$

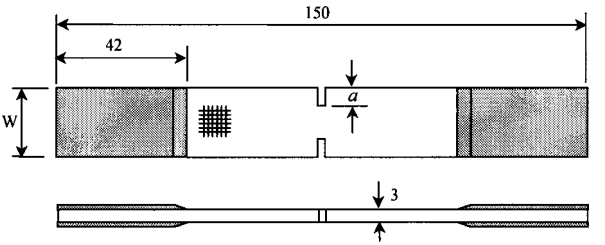

a) Tensile DEN specimen

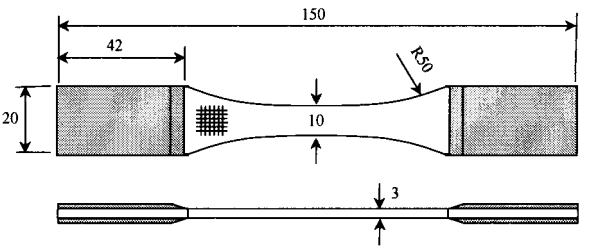

b) Tensile smooth specimen

Figure 3. Geometry and dimensions of the tensile DEN and smooth specimens.

where S_{ij} are the components of the compliance tensor.

2.4. Fracture toughness evaluation

The critical stress intensity factors of the used C/Cs were determined from the net fracture stress and the pre-crack length of the DEN specimens by use of the following equations [16]

$$K_I = \sigma\sqrt{\pi a}\, f(\xi), \tag{3}$$

$$f(\xi) = \frac{1.122 - 0.561\xi - 0.205\xi^2 + 0.471\xi^3 - 0.19\xi^4}{\sqrt{1-\xi}}, \tag{4}$$

where σ is fracture tensile stress, a is pre-crack length, and $\xi = 2a/W = 0.5$.

2.5. Finite element modeling

The loading axis COD and compliance of the CT specimens during tensile loading were determined using the finite element method (FEM) under the assumption of the plane stress condition. Figure 4 illustrates a finite element model that simulates half of the CT configuration. The mesh of this model is composed of biquadratic elements with eight nodes. In this model, a concentrated load is applied at the pinhole of the CT configuration. The material properties used in the FEM calculations are listed in Table 1. The FEM calculations were carried out using a commercial code, ABAQUS version 5.8.

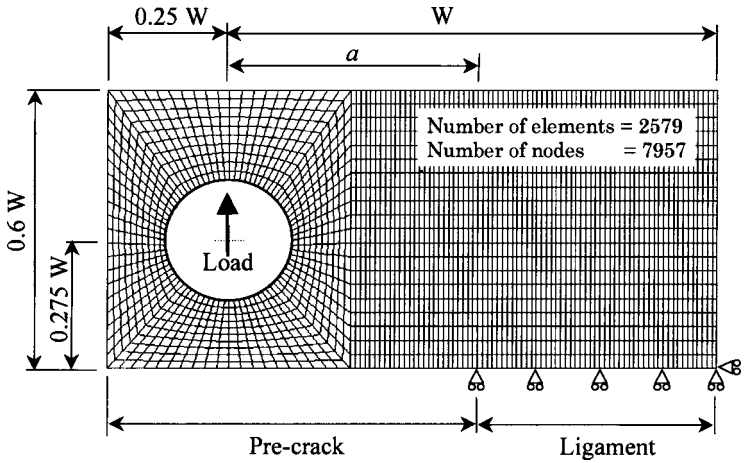

Figure 4. A finite element model for a CT specimen with $a/W = 0.5$ and $W = 50$ mm.

3. RESULTS AND DISCUSSION

3.1. Load–COD curve

Loading/unloading cycle tests were conducted to determine crack extension resistance, G_R, as a function of crack growth length using CT test specimens. Figure 5 shows a typical load–COD curve during a CT test with partial unloading. This non-complete unloading avoids excess energy dissipation in the frontal process zone [17]. It is noted in Fig. 5 that a slight non-linearity was initiated before the maximum load was applied in the first cycle, and the load dropped abruptly at the maximum load of each cycle.

3.2. Damage evolution

The CT tests demonstrated that damage growth on the surfaces of 2D-C/Cs depended on the fiber reinforcement direction (see Figs 6 and 7). For example, when the fiber reinforcement direction of the surface plies was parallel to the pre-introduced crack (90° plies), a straight crack without fiber failure extended horizontally from the pre-notch tip (Fig. 6a). On the other hand, when the surface ply fibers ran normal to the pre-introduced crack (0° plies), the initial damage observed during tensile loading in the CT samples was commonly called 'splitting' (Fig. 7a). The splitting was identified as widely opened transverse cracks. The transverse cracks were induced during the cooling stage after the processing of the C/Cs. When the applied load was increased, the splitting did not grow; however, many micro-cracks appeared between the splits in the 0° ply, as shown in Fig. 7b. Micro-cracks were located near ends of 0° ply splitting and on splitting in the adjacent 90° plies, as shown in Fig. 7c. This tendency indicated that the micro-cracks were induced by stress concentration due to a combination of splitting in the 0° ply and the adjacent 90° ply. With a further increase in load, the number of micro-

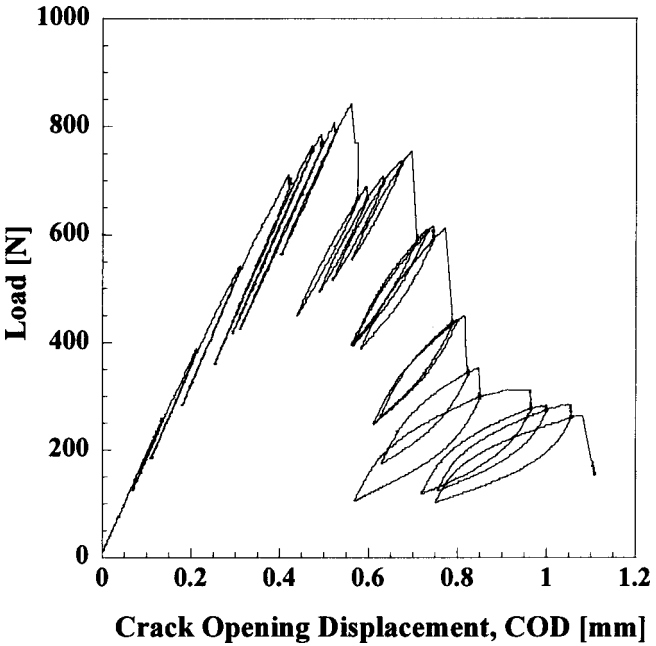

Figure 5. Relationship between load and crack opening displacement in a CT test of a 0°/90° C/C composites.

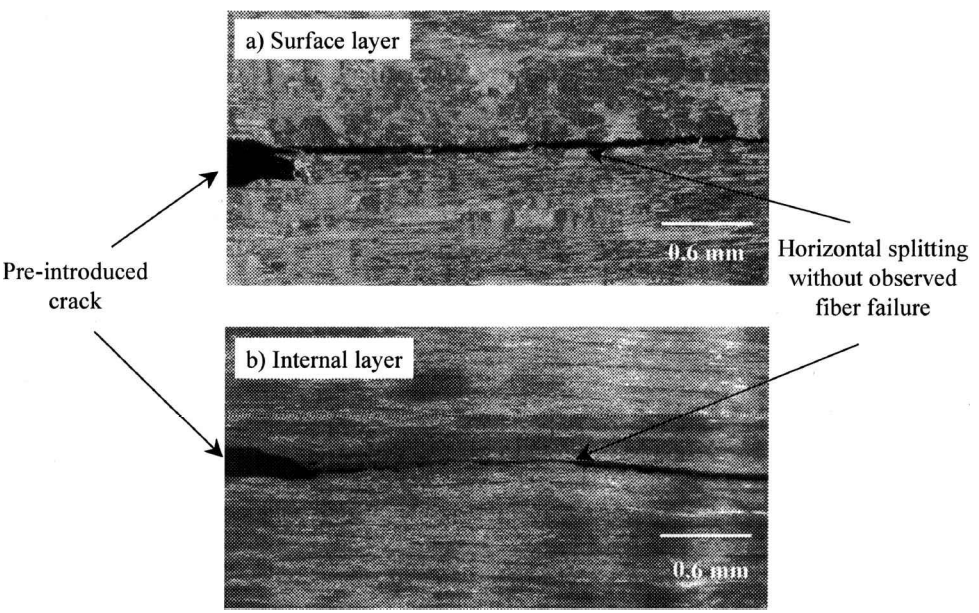

Figure 6. Damage extension in 90° plies of CT specimen. (a) 90° surface plies, (b) 90° internal plies.

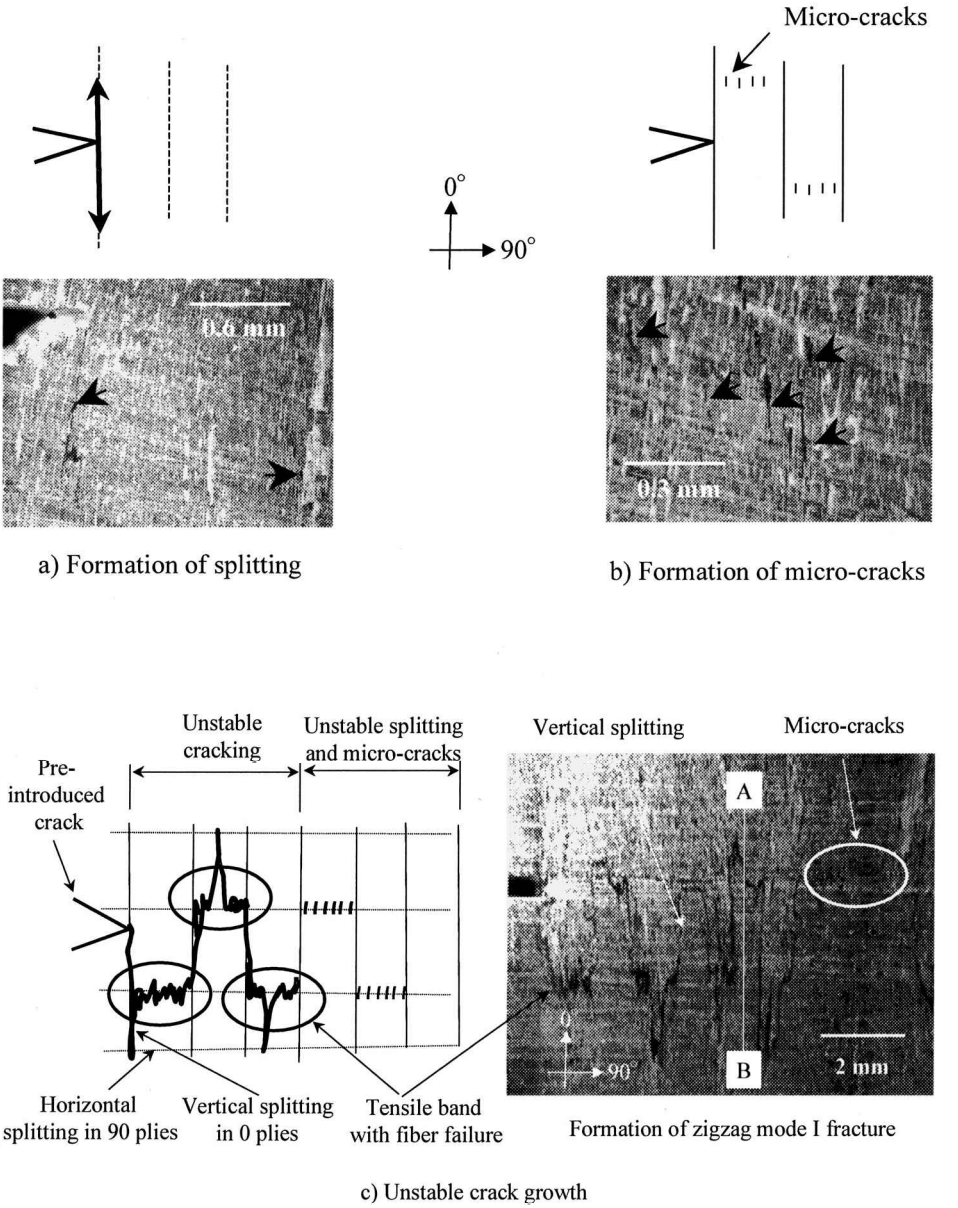

Figure 7. Damage extension in 0° plies of a CT specimen. (a) Formation of splitting; (b) formation of micro-cracks; and (c) unstable crack growth.

cracks increased, and the splitting in a 0° ply and micro-cracks eventually joined to form a large crack extension that included fiber fracture. This extension facilitated additional formation of splitting and micro-cracks ahead of the large crack, as shown in Fig. 7c. By repeating this process, fiber fracture extended across the ligament. Thus, unstable macro-zigzag cracking occurred.

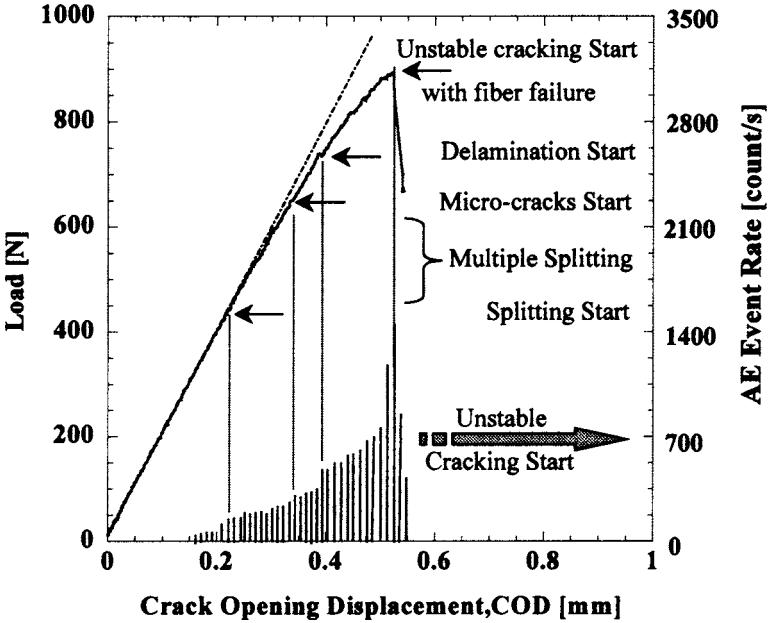

Figure 8. Acoustic-emission (AE) event rates and load as a function of crack opening displacement for the first loading of a cyclic CT test of 0°/90° C/Cs.

Figure 8 depicts the applied load and the acoustic-emission (AE) event rates as a function of crack opening displacement during the first loading of a cyclic CT test. It should be noted that in this figure, the multiple splitting gave rise to a non-linear load–COD relationship, and unstable crack growth induced a rapid load drop.

In order to reveal the damage pattern in the interior plies, the tested CT specimens were sectioned along line A-B in Fig. 7c and polished with 3 μm diamond paste. Then, the microstructures of the cross-sections were observed using a polarized light optical microscope, as shown in Fig. 9. It follows from Fig. 9 that the cracks in the 0° and 90° plies passed individually through nearly the same vertical locations and they were connected by inter-laminar delamination between the 0° and 90° plies. This result indicated that the zigzag cracks had formed in all of the 0° plies, whereas in all of the 90° plies straight splitting prevailed, parallel to the pre-crack direction.

3.3. R-curve

An apparent R-curve (Fig. 10) was obtained by applying the compliance approach. The crack growth length in this figure was determined from the 90° surface plies. This figure shows that fracture resistance rapidly increased from the initiation value of 7.6 MPa $m^{1/2}$ to a saturation value of about 20 MPa $m^{1/2}$.

As regards the zigzag crack growth, it appears necessary to take into account the influence of the cyclic stable/unstable transition of crack extension on the R-curve, because the 0° plies sustained most of load. Thus, 0° plies were the focus of the

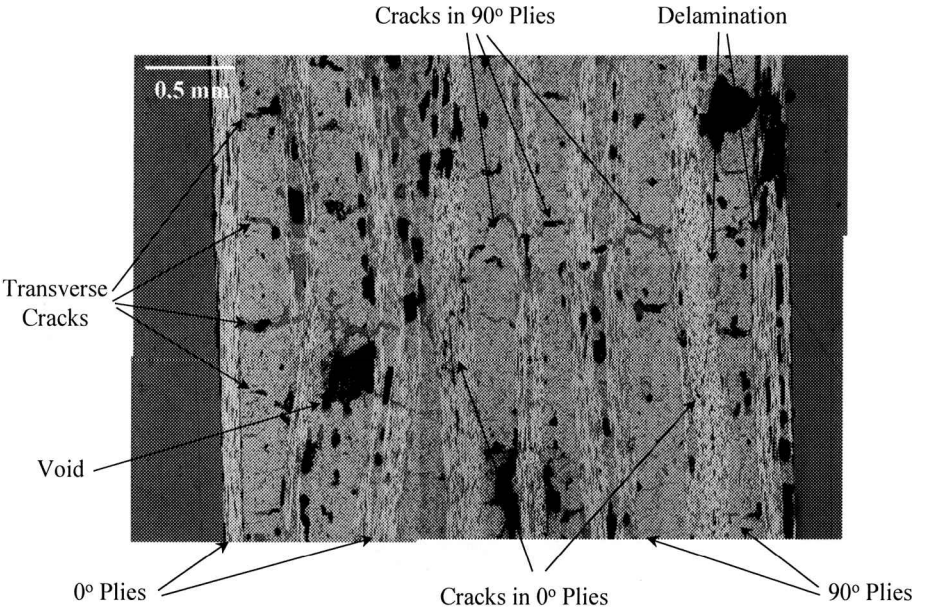

Figure 9. Micro-topography of internal damage, viewed normally to pre-introduced crack through section A-B in Fig. 7.

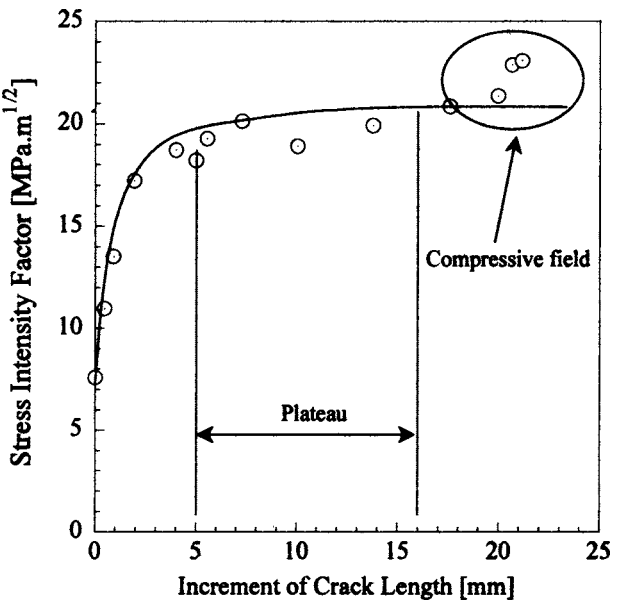

Figure 10. Crack extension resistance (R-) curve for mode I fracture of 0°/90° C/Cs based on damage in 90° ply as a function of crack growth length.

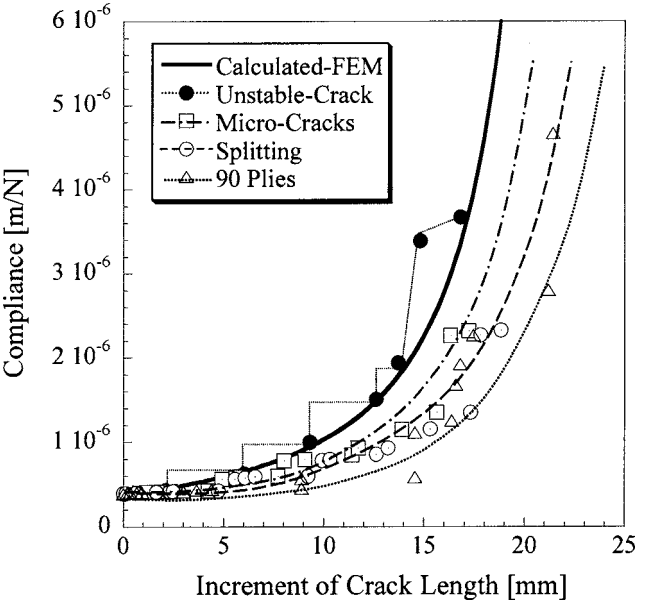

Figure 11. Compliance of 2D-C/Cs as a function of crack lengths based on initiation of splitting, micro-cracks, and unstable crack. The experimental values are compared with FEM calculated lengths.

study. Figure 11 shows compliance as a function of crack length in the 0° and 90° plies, where crack length was determined by the observed splitting in the 0° and 90° plies, by the micro-cracks, and by the unstable-crack in 0° ply. In this figure, the calculated crack lengths are also shown. Only a small fraction of the 0° fibers might have failed during the micro-crack growth; however, all of the fibers fractured during unstable crack growth. To evaluate which crack front was better for use in the determination of the R-curve, the initiations of the micro-cracks and the unstable crack, illustrated in Fig. 11, were chosen. The resulting R-curves are shown in Fig. 12. It became obvious that crack extension, based on the micro-crack, yielded a periodically fluctuating R-curve. In the first cycle, fracture resistance, based on the micro-crack, rapidly increased from the initiation value of 9.7 MPa $m^{1/2}$ to a maximum value of about 20 MPa $m^{1/2}$. From the next cycles, the initial values were higher than of that of the first cycle. This difference of the initial values is due to existence of splits and micro-cracks at the initial stages of the subsequent higher cycles. In the case of the unstable R-curve, as shown in Fig. 12, the initial and saturated values were almost similar to the maximum value of the micro-crack R-curve, i.e. no rising R-curve was observed for an unstable R-curve representation. This finding indicated that the rising R-curve, high fracture toughness, in 2D-C/Cs was yielded during the micro-crack formation concomitant with zigzag damage.

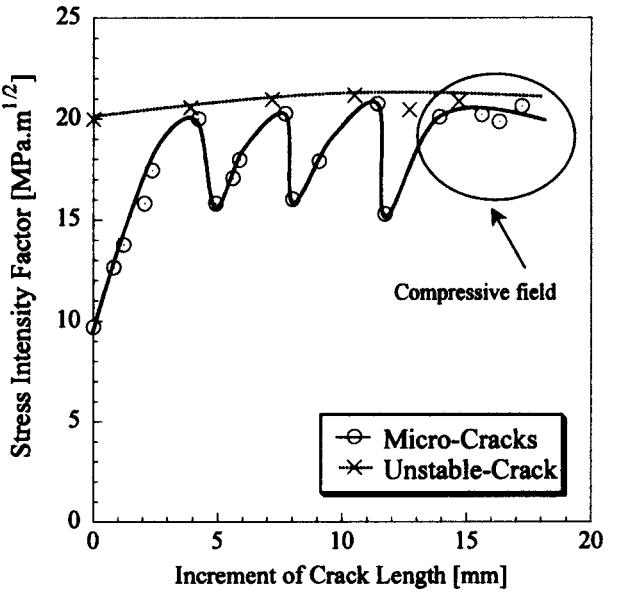

Figure 12. Zigzag R-curves based on micro-cracks and unstable crack growth in 0° plies as a function of the tensile growth band of a zigzag crack.

3.4. Fracture toughness criterion

The net tensile fracture stresses of the DEN specimens versus the pre-crack lengths are shown in Fig. 13. This figure shows clearly that the fracture stress was higher or lower than that of the averaged stress of the smooth specimens when the pre-crack length is short or long, respectively. The averaged stress of the smooth specimens was determined in over 10 specimens and was confirmed to be independent of specimen width [14]. In Fig. 13, the dotted and dashed lines were determined by the fracture toughness criterion using the initial values of both R-curves that had been obtained based on the crack extension lengths of the 90° and 0° (micro-cracks in the zigzag cracking) surface plies, respectively. The best fit obtained by the fracture toughness criterion with the experimental DEN results, solid line, was yielded at a stress intensity factor of 11 MPa $m^{1/2}$. This value was slightly higher than the crack extension resistance based on micro-crack growth (zigzag crack). Precisely, fracture of materials should be determined using the entire R-curve as has previously been discussed by Broek [18]. This approach should resolve this slight discrepancy.

From the above results, it can be concluded that the splitting and micro-cracks formation during the zigzag cracking is effective toughening mechanism controlling the fracture of DEN specimens. However, the splitting and micro-cracks are small-scaled and slight damage. This is why we could not identify the damage near the crack tips of the DEN specimens in the previous reports [13, 14].

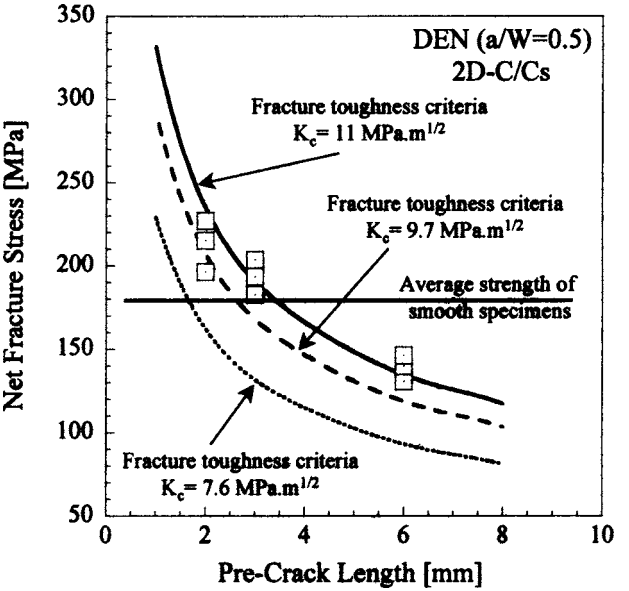

Figure 13. Net fracture stress of DEN specimens as a function of pre-crack length.

4. CONCLUSIONS

The main conclusions of the present study are as follows.

(1) Zigzag cracking occurred in 0° plies in cross-ply C/C composite. One cycle of zigzag cracking proceeded in the following order, i.e. at first, vertical splits were observed, then micro-cracks between those splits, and finally unstable crack growth connected the micro-cracks and splits.

(2) This stable/unstable regime of zigzag cracking was repeated.

(3) A zigzag R-curve represented the intrinsic toughness of cross-ply laminated C/C composites.

(4) The high-fracture toughness of the cross-ply laminated C/C composites was attributed to the zigzag cracking characteristics.

(5) Matrix cracks induced either upon processing or during testing were found to have a strong influence on the toughening mechanism of the cross-ply laminated C/C composites.

Acknowledgements

This study was partly supported by Grants-in-Aid for Basic Science (grant No. 11305047) from the Ministry of Education, Sports, Culture, Science and Technology of Japan.

REFERENCES

1. C. R. Thomas, *Essentials of Carbon-Carbon Composites*. The Royal Society of Chemistry, Cambridge, England (1993).
2. G. Savage, *Carbon-Carbon Composites*. Chapman and Hall, New York, NY (1993).
3. E. Fitzer and L. M. Manocha, *Carbon Reinforcements and Carbon/Carbon Composites*. Springer-Verlag, Berlin, Germany (1998).
4. D. L. Schmidt, K. E. Davidson and S. Theibert, Unique applications of carbon-carbon composite materials (Part One), *SAMPE J.* **35** (3), 27–39 (1999).
5. D. L. Schmidt, K. E. Davidson and S. Theibert, Unique applications of carbon-carbon composite materials (Part Two), *SAMPE J.* **35** (4), 51–63 (1999).
6. D. L. Schmidt, K. E. Davidson and S. Theibert, Unique applications of carbon-carbon composite materials (Part Three), *SAMPE J.* **35** (3), 47–55 (1999).
7. A. Wanner, G. Rizzo and K. Kromp, in: *Toughening Mechanisms in Quasi-brittle Materials*, S. P. Shah (Ed.), pp. 405–423. Kluwer Academic Publishers, London (1991).
8. A. G. Evans and F. W. Zok, Review: The physics and mechanics of fiber-reinforced brittle matrix composites, *J. Mater. Sci.* **29**, 3857–3896 (1994).
9. J. W. Cao and M. Sakai, The crack-face fiber bridging of a 2D-C/C-composites, *Carbon* **34** (3), 378–395 (1996).
10. F. E. Heredia, S. M. Spearing, T. J. Mackin and A. G. Evans, Notch effects in carbon matrix composites, *J. Am. Ceram. Soc.* **77** (11), 2817–2827 (1994).
11. T. J. Mackin, T. E. Purcell, M. Y. He and A. G. Evans, Notch sensitivity and stress redistribution in three ceramic-matrix composites, *J. Am. Ceram. Soc.* **78** (7), 1719–1728 (1995).
12. C. Cady, E. Heredia and A. G. Evans, In-plane mechanical properties of several ceramic-matrix composites, *J. Am. Ceram. Soc.* **78** (8), 2065–2078 (1995).
13. H. Hatta, Y. Kogo, H. Asano and H. Kawada, Applicability of fracture mechanics in carbon-carbon composites, *JSME Int. J., Series A* **42** (2), 265–271 (1999).
14. Y. Kogo, H. Hatta, H. Kawada and T. Machida, Effect of stress concentration on tensile fracture behavior of carbon-carbon composites, *J. Compos. Mater.* **32** (13), 1273–1294 (1998).
15. G. Chollon, O. Siron, J. Takahashi, H. Yamauchi, K. Maeda and K. Kosaka, Microstructure and mechanical properties of coal tar pitch-based 2D-C/C composites with a filler addition, *Carbon* **39**, 2065–2075 (2001).
16. H. Tada, P. C. Paris and G. R. Irwin, in: *The Stress Analysis of Cracks Handbook*, pp. 2.6–2.7. Del Research Co., Pennsylvania (1973).
17. M. Sakai and R. C. Bradt, Fracture toughness testing of brittle materials, *International Materials Reviews* **38** (2), 53–77 (1993).
18. D. Broek, in: *The Practical Use of Fracture Mechanics*, pp. 79–86. Kluwer Academic Publishers, The Netherlands (1988).